

Monoclinic tungsten trioxide (WO₃) thin films using spraying pyrolysis: electrical, structural and stoichiometric ratio at different molarity

F. A. Mohamed, E. T. Salim*, A. I. Hassan

Laser Science and Technology Branch, University of Technology - Iraq, Baghdad, Iraq

Chemical spraying pyrolysis technique has used to deposit tungsten oxide on glass substrates with varied concentrations ranging from 50 to 90 mM at the optimum deposition temperature of 350 °C. All films exhibit a monoclinic phase, with highest structural properties at a molar concentration of 80 mM. Miller's plain at (200) was found to be the most dominant in all films. The film has a fibrous network with an increasing diameter with increasing concentration, according to FE-SEM. The EDX revealed that the ratio of W/O at the optimum concentration (80mM) was 2.62, with a stoichiometric of 68.6%. The rate of grain size grew with concentration, whereas the rate of roughness reduced with concentration, according to atomic force microscopy investigations of thin films. The mean electrical conductivity increased gradually with concentration up to $4.176 \times 10^{-8} \text{ S/cm}^{-1}$ and subsequently declined to $4.542 \times 10^{-10} \text{ S/cm}^{-1}$, while the activation energy climbed gradually with concentration up to reach 0.298eV before decreasing significantly.

(Received March 22, 2022; Accepted September 16, 2022)

Keywords: tungsten trioxide; monoclinic structure; spraying pyrolysis, electrical properties; stoichiometric ratio.

1. Introduction

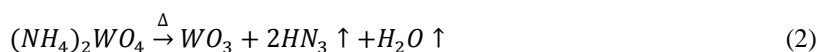
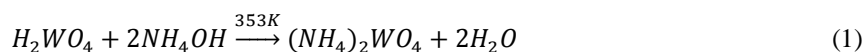
TCOs with wide band gaps, such as Zinc oxide (ZnO), tungsten trioxide (WO₃), Niobium pentoxide (Nb₂O₅), and hafnium dioxide (HfO₂), show substantial commercial promise in the manufacturing of opto-electronic devices due to their distinctive properties [1-3]. Wide band gaps materials outperform other materials in terms of electrical characteristics and free-electron velocities, making them ideal for large power switching devices and radio wave applications[4-9]. Electronic devices (diodes, transistors, photodetectors, and capacitors) now have the ability to function at greater voltages, frequencies, and temperatures thanks to these materials (above 250 C) [10-12]. Many research communities have been intrigued by these odd traits over the years, encouraging them to look into their scientific and technical implications, particularly in semiconducting devices [13, 14]. WBG-TMO tungsten trioxide (WO₃) is a multifunctional material with a number of distinguishing characteristics, including sharp phase transformation, a large band gap (2.6- 3.6 eV), high crystallinity, and an effective surface structure [15-18]. This (TMO) transition metal oxide is abundant in nature, cheap, non-toxic to living things, and eco-friendly [19, 20]. The potential application of WO₃ as a ferroelectric, or catalyst, in smart electrochromic windows, gas sensors, and optical devices has sparked a lot of interest [21-27]. A vary of techniques have been used to make WO₃ thin films, including chemical vapour deposition [28], hydro-thermal[29], reactive-magnetron sputtering [30], and spray pyrolysis [31]. SPT (chemical spray pyrolysis method) is a low-cost approach with a simple experimental setup, great homogeneity, a broad coating area, and high product purity. Temperature, air pressure, and solution volume can all be changed throughout the film deposition process [32-34].

For different solution concentrations, including 50mM, 60mM, 70mM, 80mM, and 90mM, the SPT technique was employed to make WO₃ thin films. The structural, morphology, and electrically characterizations of WO₃ films were studied using XRD, FE-SEM, Energy dispersive X-ray (EDX), and electrical conductivity.

* Corresponding author: evan.t.salim@uotechnology.edu.iq
<https://doi.org/10.15251/DJNB.2022.173.1029>

2. Experimental details

To manufacture WO₃ thin films, a spray pyrolysis procedure was utilized. The spraying equipment was made at home as an experiment. The spray solution was prepared by mixing pure tungstic acid (H₂WO₄) powder (Merck) in ammonium hydroxide (NH₄OH) at 353K for 10 minutes while stirring in exactly 50 ml for all of the films. The chemical reaction in question is as follows: [35].



From 50mM to 90 mM, the concentration of the precursor solution was adjusted in 10mM increments. An air compressor was employed to atomize the solution. The distance between the nozzle and the substrate was kept at 28.5 cm, and the temperature of the substrate was set at 350°C and held within 10°C using a temperature control device on the hot plate's metal surfaces. The 2cm X 2cm substrate was constructed of glass that had been preheated to the proper temperature before being sprayed on.

3. Results and discussion

The structural alterations and phase of as-synthesised WO₃ thin films are investigated using an X-Ray pattern. The XRD patterns of all WO₃ thin film samples placed on glass substrates are shown in Figure 1, at an optimised temperature of 350°C with various molarity concentrations (50 – 90) mM increments of 10 mM. All XRD peaks were attributed to the monoclinic phase of WO₃, indicating its pristine crystal structure in the absence of secondary or impurity phases (JCPDS Card No.43-1035)[36]. The XRD pattern displays a well-defined peak triplet that may be classified as (002), (020), and (200) at $2\theta = 23.21, 23.68,$ and $24.19,$ respectively, and is attributed to monoclinic WO₃ with preferred orientation along the (200) plane. The peak place is shown to be independent of molarity concentration, but peak intensity is. Peak intensity rises as molarity rises, indicating a rise in the crystalline component of the films. As solution concentrations rise to 90 mM, the strength of the (200) peak increases, then gradually drops. This is due to the production of a powdery substance that may be readily wiped away, making the film's surface less sticky[37]. Several diffraction peaks with lower intensities have been recorded at 2θ values of 28.103, 33.917, 41.819, 49.658, and 55.517, corresponding to the (hkl) planes (-112), (202), (222), (400), and (-142)[22]. Peak intensity is linked to crystallinity, however film thickness can also play a role [38].

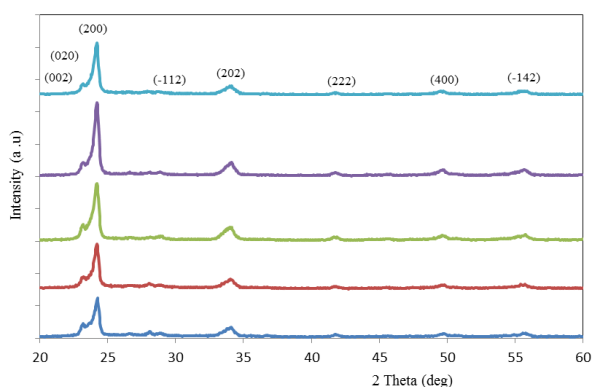


Fig. 1. X-ray pattern of WO₃films for different concentrations.

Scherer's well-known Debye formula[39-42] The crystalline size values were calculated using this method. Table of contents (1) demonstrates how the structural characteristics of WO₃ thin films change over time.

$$D = \frac{0.9\lambda}{\beta \cos\theta} \quad (3)$$

where D is the crystallite size, and $\lambda = 0.154056$ nm is the wavelength of the Cuka line, β the full width at half maximum for the corresponding peak, and the Bragg's angle in radians. Table 1 shows the variation in crystallite size as a function of concentration. The observed crystallite size trend is consistent with the thickness of the film [43]. D values are lower for thin layers and greater for bigger layers. The smaller crystallite size at lower thicknesses could be owing to a higher interaction between the substrate and the vapour atoms, which affects both ad-atoms and subcritical nuclei mobility [44]. The film precipitate with an 80 mM concentration of the solution has the highest D value, as well. The strength of the peaks increases as the concentration rises, increasing the crystallinity [45]. The D values were shown to decrease as the molarity concentration rose up to 90mM, which is attributable to grain coalescence and nucleation [46] Micro strain measurements are a critical component in establishing the mechanical stability of films. Equations (4), (5), and (6) were used to compute microstrain, density of dislocations (δ), and stacking fault (SF) (6) [35, 47-51] shown in table (1)

Table 1. WO_3 thin film structural properties at various concentration.

Molarity Concentration	2 θ ($^\circ$)	hkl	d (Å)	FWHM (rad)	D (nm)	δ $\times 10^{14}$ lines m^{-2}	$\epsilon \times 10^{-3}$ lines $^{-2}$ m^{-4}	SF $\times 10^{-2}$	TC
50	23.25	002	3.82198	0.00964	14.70	4.62508	0.23622	0.310	0.9677
	24.16	200	3.68015	0.00914	15.49	4.16656	0.22346	0.288	0.9874
	28.85	-112	3.09185	0.01039	13.49	5.49506	0.25173	0.299	1.0117
	33.90	202	2.64151	0.01514	9.14	1.19475	0.36210	0.400	1.0239
	41.76	222	2.16115	0.00989	13.68	5.34306	0.23105	0.233	1.0076
	49.63	400	1.83511	0.01221	10.76	8.62901	0.27710	0.262	1.0259
	55.70	214	1.64874	0.00996	12.85	6.05038	0.22020	0.200	0.9755
60	23.25	002	3.82198	0.00907	15.63	4.08955	0.22212	0.292	1.0685
	24.18	200	3.67728	0.00802	17.64	3.21116	0.19616	0.253	0.9800
	28.10	-112	3.17296	0.00746	18.81	2.82436	0.18107	0.218	0.8968
	34.07	202	2.62875	0.01006	13.75	5.28419	0.24060	0.265	1.0426
	41.76	222	2.16111	0.00893	15.15	4.35679	0.20863	0.211	0.9515
	49.64	400	1.84943	0.01022	12.85	6.04743	0.23197	0.219	1.0363
	55.51	-142	1.65390	0.01433	8.93	1.25171	0.31726	0.288	1.0239
70	23.21	002	3.82848	0.00758	18.69	2.86144	0.18583	0.244	0.9985
	24.19	200	3.67511	0.00866	16.33	3.74871	0.21194	0.273	1.0013
	28.10	-112	3.17255	0.00704	19.93	2.51653	0.17092	0.205	0.9012
	33.91	202	2.64089	0.01528	9.065	1.21692	0.36544	0.404	0.9613
	41.81	222	2.15834	0.00882	15.32	4.25686	0.20615	0.208	1.1682
	49.65	400	1.83442	0.01081	12.15	6.77046	0.24542	0.232	1.0681
	55.66	214	1.64973	0.01242	10.31	9.4043	0.27462	0.249	0.9012
80	23.21	002	3.82848	0.00781	18.15	3.03503	0.19138	0.251	0.9508
	24.19	200	3.67529	0.00760	18.61	2.88496	0.18592	0.240	0.9418
	28.84	112	3.09237	0.00778	18.02	3.07709	0.18838	0.224	0.9314
	33.97	202	2.63617	0.01353	10.23	9.55259	0.32366	0.357	1.0795
	41.73	222	2.16270	0.00999	13.53	5.45558	0.23352	0.236	1.0779
	49.61	400	1.83592	0.01046	12.56	6.33851	0.23754	0.224	1.0182
	55.70	214	1.64874	0.00976	13.10	5.81951	0.21595	0.196	0.9508
90	23.21	002	3.82848	0.00812	17.45	3.28381	0.19907	0.262	0.3706
	24.16	200	3.68061	0.00821	17.23	3.3663	0.20086	0.259	1.5608
	33.98	202	2.63601	0.01397	9.91	1.01782	0.33409	0.369	0.9989
	41.76	222	2.16083	0.01032	13.10	5.82485	0.24123	0.244	1.0405
	49.57	400	1.83719	0.01304	10.07	9.84823	0.29618	0.280	0.9364
	55.54	-142	1.65302	0.01582	8.09	1.52441	0.35002	0.318	1.0925

$$\varepsilon = \frac{\beta \cos \theta}{4} \quad (4)$$

$$\delta = \frac{1}{D^2} \quad (5)$$

$$SF = \left[\frac{2\pi^2}{45(3 \tan \theta)^2} \right] \beta \quad (6)$$

$$TC = \frac{I_o(h_i k_i l_i)}{I_s(h_i k_i l_i)} / \left[\frac{1}{N} \sum \frac{I_o(h_i k_i l_i)}{I_s(h_i k_i l_i)} \right] \quad (7)$$

With the rise of solution concentration to 80 mM, the predicted micro-strain, dislocation density, and stacking faults all decreased (Table 1). For higher solution concentrations up to 80 mM, the decrease in micro-strain, dislocation density, and stacking defects suggests that the films' crystallinity has improved. This reduction in microstrain, dislocation density, and stacking faults implies a reduction in lattice defects along grain boundaries, as well as change in interplanar spacing of the films [52, 53]. Table 1 shows the results. One of the basic structural properties of poly-crystalline materials is the coefficient of texture. By using Equation (7) [54, 55]. In general, the texture coefficient (TC) for a film with a preference orientation in any (hkl) plane must be at least 1. As shown in the table, the value of TC for the majority of the films made at various concentrations is equal to one (1). This suggests that tungsten oxide coatings develop preferentially [47, 52].

FE-scanning electron microscopy was used to examine the morphology of WO₃ thin films in Figure 3. At 350 degrees Celsius, the varied concentrations (50 mM - 90 mM) were deposited on the glass substrate. Inside is the cross section for films. Regardless of the spray solution dosage, all of the FE-SEM images had a nearly identical shape. The varying fibre sizes may be seen in the WO₃ thin film samples. Furthermore, for solution concentrations of 50 mM, 60 mM, 70 mM, 80 mM, and 90 mM, the WO₃ thin films have a fibrous reticulated structure with an average fibre width of 88, 133, 152, 266 and 115 nm, respectively. This may be supported by study [38]. This image exhibits FE-SEM images of varying concentrations of WO₃ thin films. The film's fibre network begins to grow at 50 mM. There are also random nanoparticles with a diameter of 22 nanometers, and the fibre diameter grows as the solution concentration rises to 80 mM, then declines at 90 mM, as seen above. At 60 mM, the interior network of fibres begins to expand, with various fibre diameters visible. This was caused by fine droplets colliding and decomposing on the substrate, As the solution concentration rises, the disintegration and overlapping of droplets occurs again [31]. There were also nanoparticles with sizes of 39nm and 32nm at 60mM and 70 mM, respectively; however, no nanoparticles were seen at (80-90) mM, only a fibre network with internal fibre networks with diameters of 70-100nm. The films appear to be made up of several layers of fibrous material [56].

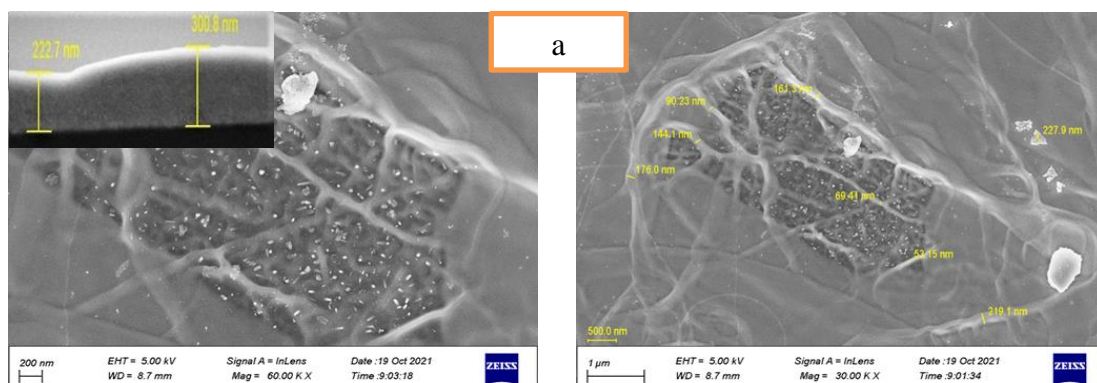


Fig. 2.1. Shown FE-SEM and cross section of WO₃ thin films at substrate temperature 350°C, and different concentration: a=50mM

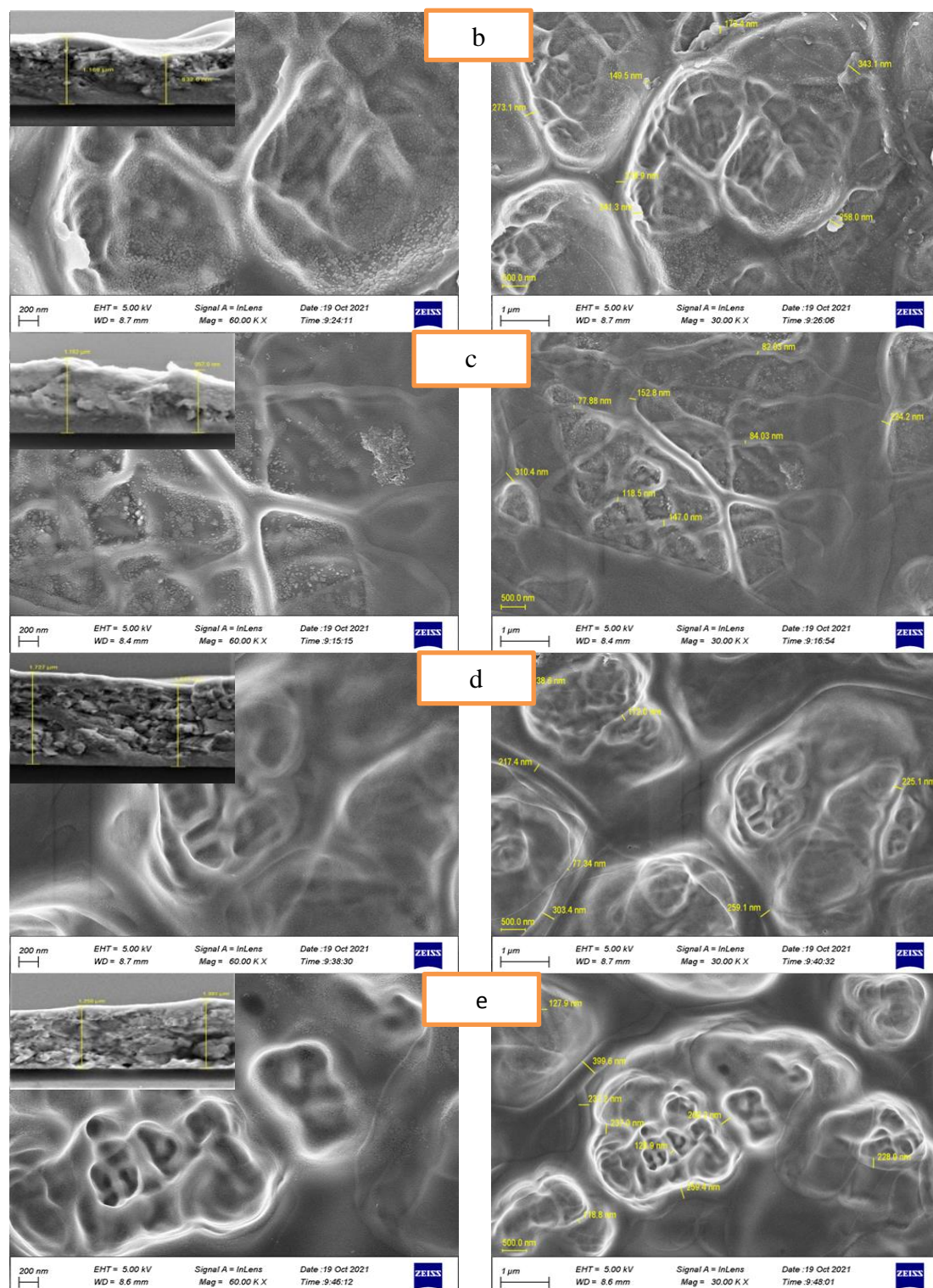


Fig. 2.2 Shown FE-SEM and cross section of WO_3 thin films at substrate temperature 350°C , and different concentration (b=60mM, c=70mM, d=80mM, e=90mM).

Figure 3 depicts the EDX scale of spray-placed WO_3 nanofibers at various mole concentrations (50, 60, 70, 80, and 90) mM. The presence of the expected elements tungsten (W) and oxygen (O), as well as the absence of any undesired impurities, can be seen in the spectrum. The atomic percent fluctuations of WO_3 films layered with various mole concentrations on a 350°C substrate are summarised in Table 2. The number of W atoms in films increased as the mol concentration of WO_3 increased, but the number of O atoms decreased till 80 mM. The trend was

reversed when the mole concentration was increased to 80-90 mM of WO_3 . For 80 mM of WO_3 nanofiber films, the greatest value of W and the smallest value of O were achieved. It is clear that a lack of oxygen could result in improved electrical conductivity for WO_3 film. The trend was reversed when the concentration of molarity was increased to 80-90 mM of WO_3 . For 80 mM of WO_3 nanofiber films, the greatest value of W and the smallest value of O were achieved. It is clear that an oxygen deficiency could result in improved electrical conductivity for WO_3 film, regular with the XRD results and FE-SEM results.

Table 2. Atomic percentage of the WO_3 thin films at different concentration.

Mole concentration(mM)	Atomic ratio(%)		stoichiometry (%)
	W	O	
50	11.44	88.56	41.7
60	18.47	81.53	67.7
70	18.69	81.31	68.5
80	19.47	80.53	68.6
90	17.63	82.63	66.7

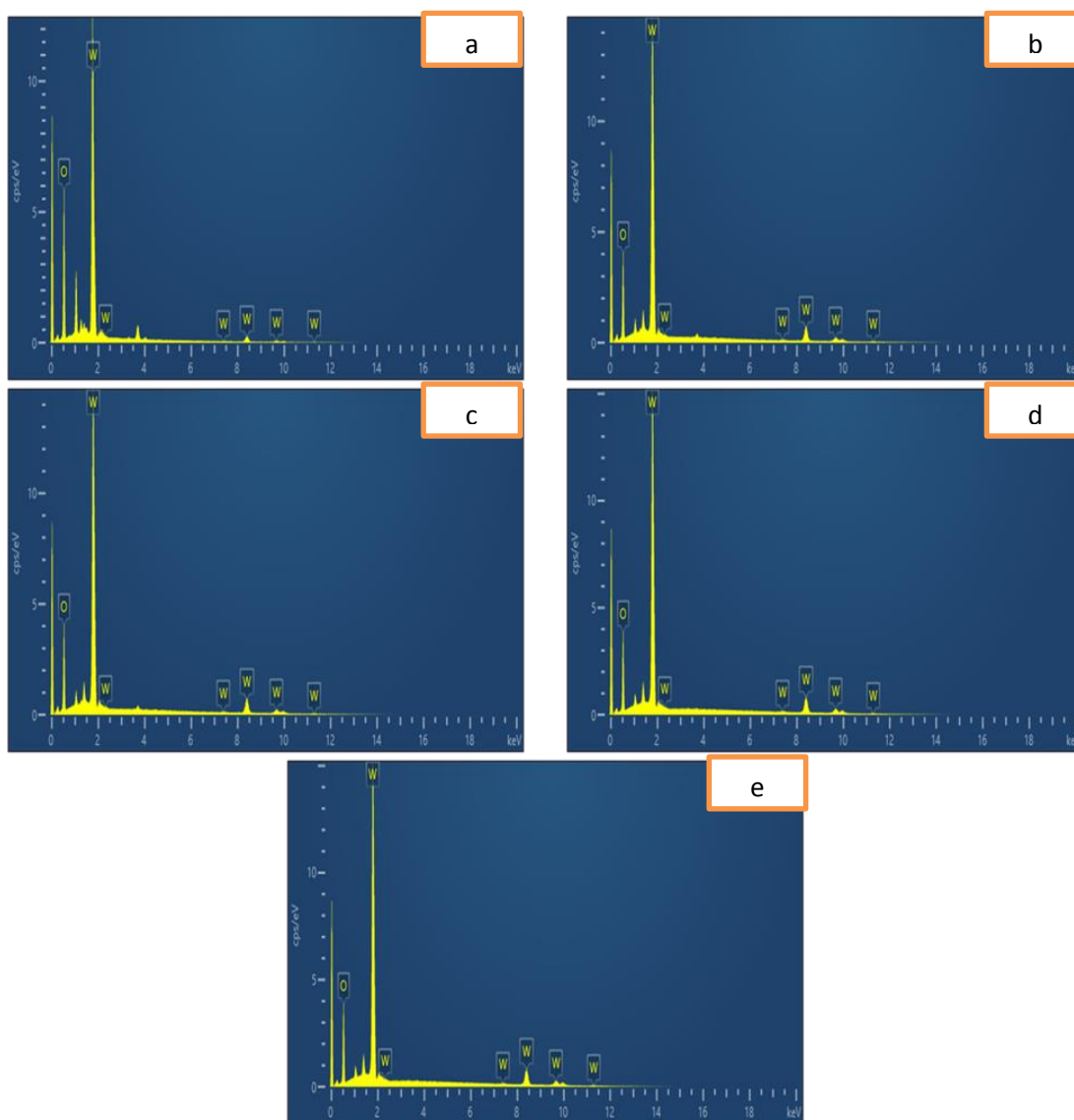


Fig. 3. EDX results of the WO_3 thin film at substrate temperature 350°C , and different concentration (a=50mM, b=60mM, c=70mM, d=80mM, e=90mM)..

AFM picture of WO_3 thin films with various molarity concentrations is shown in Figure 4. As a function concentration of solution, atomic force microscopy (AFM) pictures in a $5\text{m} \times 5\text{m}$ region are captured. The average of roughness of the WO_3 films and their particle size are listed in Table 3. With a rise in solution concentration, the particle size appears to increase. It's possible that it's due to grain agglomeration when the solution concentration rises. Because of the faster growth rate, grain agglomeration increased, resulting in non-directional grain growth on WO_3 films of various concentrations [22]. At the concentrations of (50,60,70) mM, metal oxides have a fibrous reticulate-like morphology, which is one of their distinguishing features [57]. These findings back up the findings of the FE-SEM. The surface morphology improved and mean roughness reduced as the molarity concentration increased, as indicated in table 3. The morphology of samples deposited from a higher molarity precursor solution (80mM and 90mM) is denser, with overlaid islands. When aerosol droplets collide with a solid surface, the reactant molecules lose energy and may bond to the surface, generating solitary nuclei. A continual adsorption of the droplets onto the substratum, followed by an interaction between the tungsten-containing types and the already produced nuclei, aids film formation. Following the formation of monolayer(s) on the substratum, islands form, most likely as a result of the chemical species' decreased bonding energy to the existing layers as the concentration of reactants on the surface reaches a saturation point under the chosen experimental condition (island-layer Stranski–Krastronov) mechanisms [58].

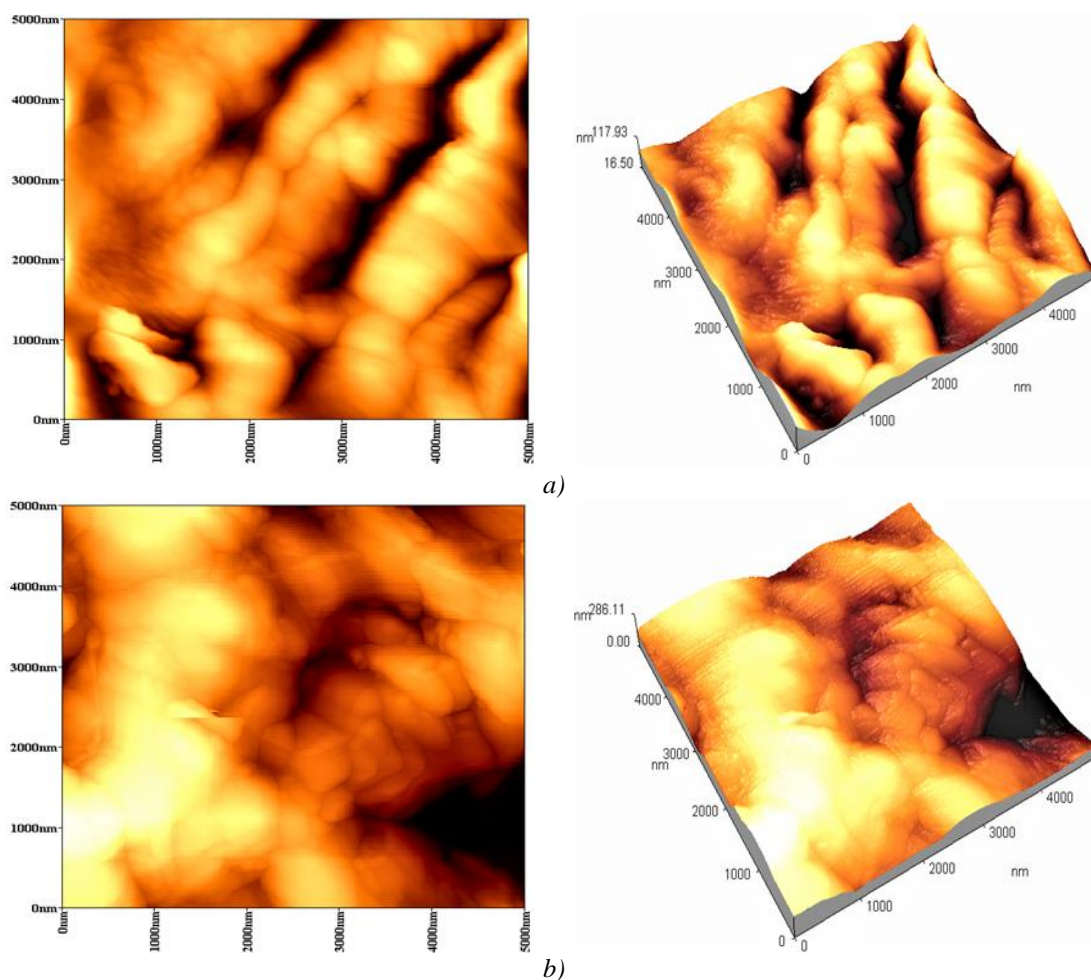


Fig. 4.1. AFM images at different concentration of the WO_3 thin films at substrate temperature 350°C , and different concentration ($a=50\text{mM}$, $b=60\text{mM}$,)

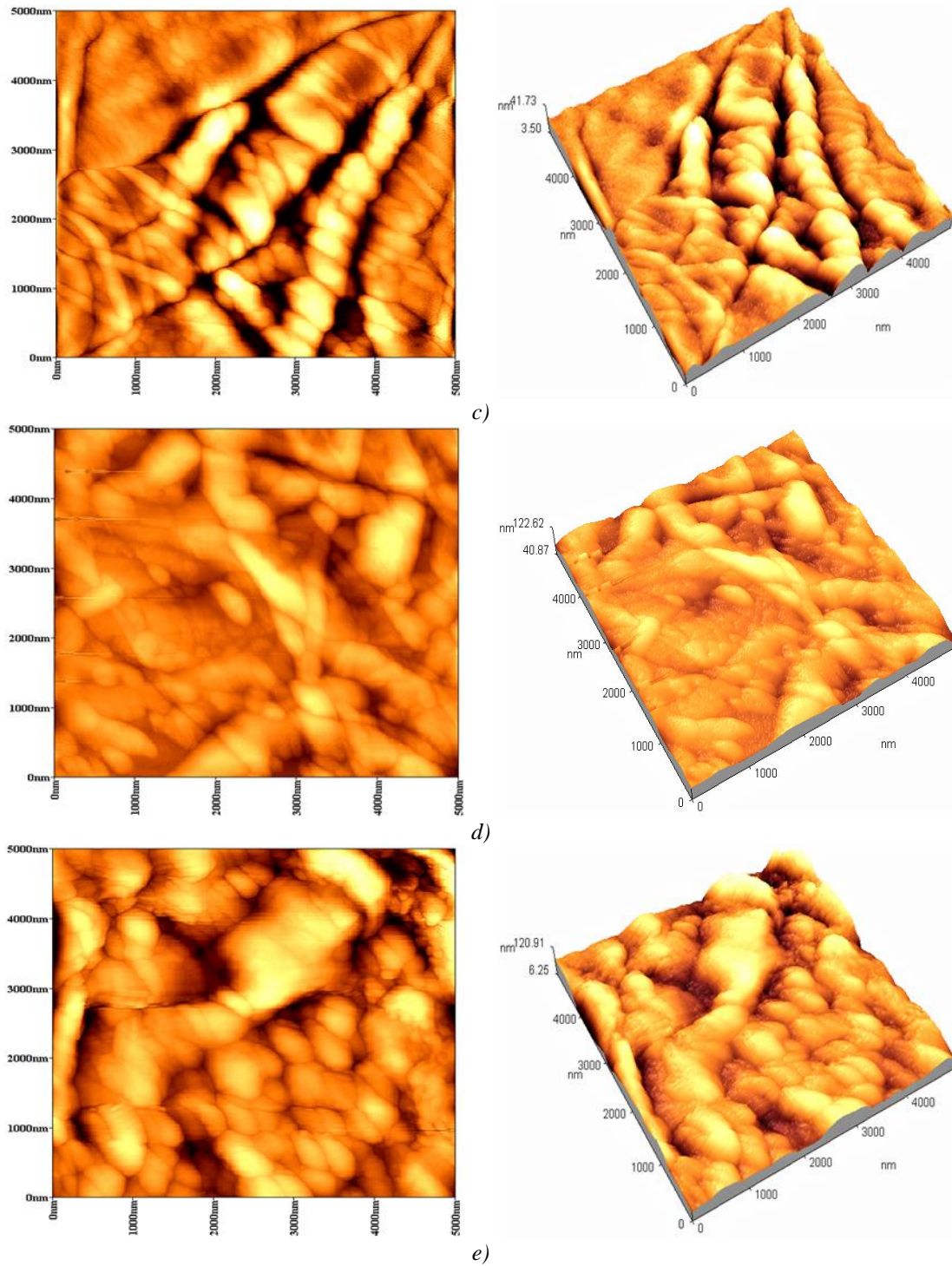


Fig. 4. AFM images at different concentration of the WO_3 thin films at substrate temperature 350°C , and different concentration ($c=70\text{mM}$, $d=80\text{mM}$, $e=90\text{mM}$).

Table 3. The avg grain size, roughness avg and root mean square of the WO₃ thin films.

Molarity concentration (mM)	Avg grain sizes (nm)	roughness Avg (nm)	Root mean square (nm)
50	80.65	30.81	38.09
60	81.35	36.92	42.79
70	82.45	33.23	40.41
80	83.09	27.46	34.57
90	71.19	27.32	33.46

The I–V features of spray covered WO₃ nanofiber films were investigated at temperatures ranging from 303 to 423, as shown in Fig.5. At various measuring temperatures, it was discovered that the experimental values of I rise linearly with applied voltage (10–100) V. The I–V characteristics demonstrate that the matching curve grew exponentially as the film's measurement temperature increased. When measured at 423K instead of 303K, the film improved and had higher I values. The level of resistance fell, When the temperature rises, extra heat energy may cause electrons to be released from the lattice for conduction [31]. Films with the least amount of oxygen in them probably performed best. When compared to other temperatures, the I values are exceptionally high at 423K[47].

The below equation was used to compute the dc electrical conductivity [59-63].

$$\sigma = \left[\frac{I}{V} \right] \times \left[\frac{d}{A} \right] \quad (8)$$

where I represents current, V represents applied potential, d represents inter-probe distance, and A represents the film's cross-sectional area. computed conductivity of deposited WO₃ thin films at varied solution concentrations The typical conductivity values for solution concentrations of 50 to 90 mM are 4.5428x10⁻¹⁰, 4.554x10⁻⁹, 1.2501x10⁻⁸, 4.1762x10⁻⁸, and 1.1964x10⁻⁸ S/cm. It also reveals that the conductivity value rises to 80 mM before falling due to the surface structure affecting the link between the O and W atoms. As a result, the concentration of oxygen vacancy in the WO₃ films decreases, resulting in a lower σ_{dc} [64]. This results was agreement with the research [59, 65]. Furthermore, as the molar concentration rises, an increase in film thickness can improve the crystalline size of the thin film, resulting in a decrease in trapping states at grain boundaries and an increase in carrier mobility, as well as an increase in film thickness, resulting in an increase in carrier concentration [66, 67].

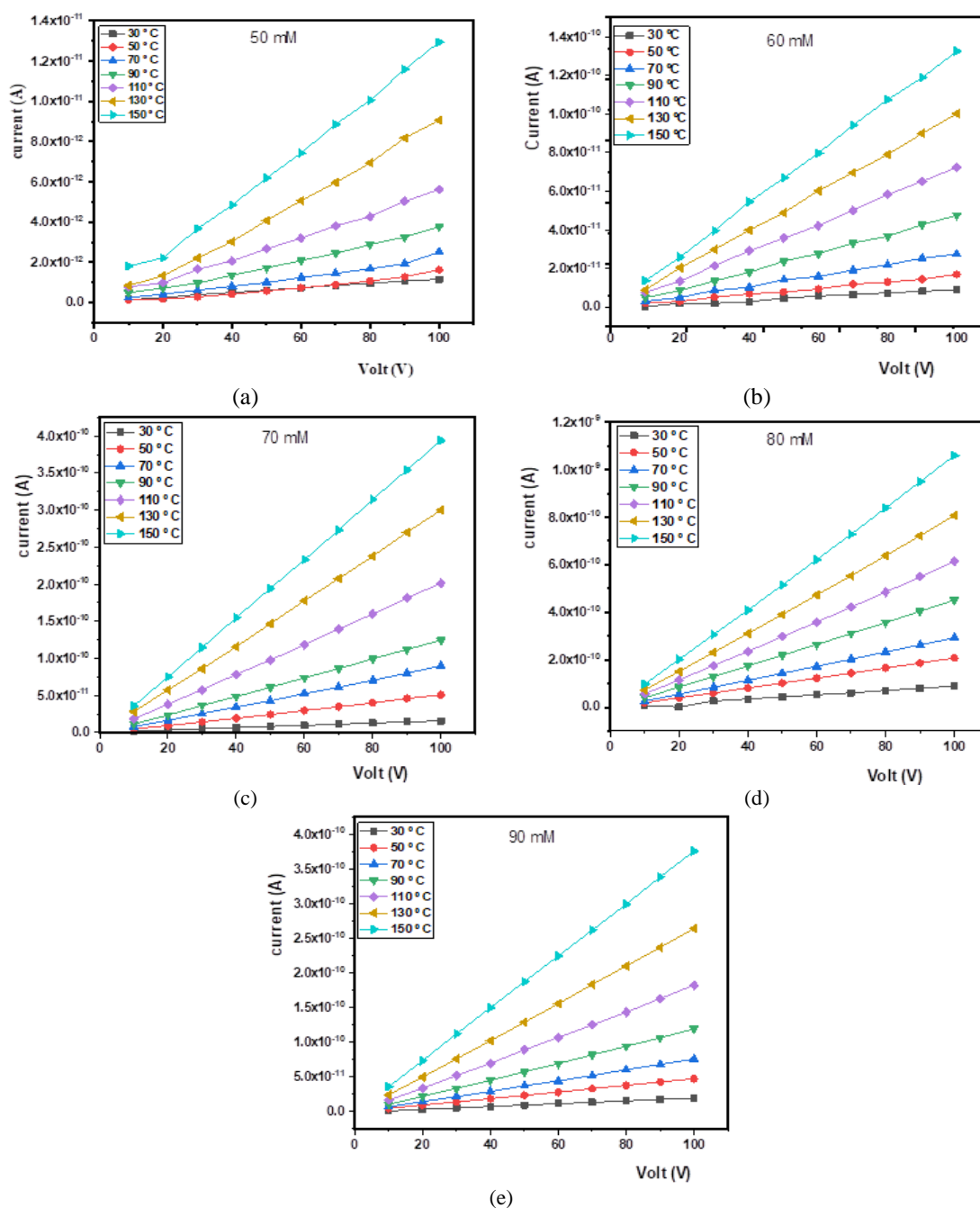


Fig. 5. I-V characterization of WO₃ thin films at substrate temperature 350°C, and different concentration (a=50mM, b=60mM, c=70mM, d=80mM, e=90mM).

The electrical properties of WO₃ films made at various molarity concentrations are listed in Table 4. The electrical resistivity (ρ) of the films declined steadily with molarity concentration (50-80) mM and subsequently increased at 90mM, yielding (ρ) values of (2.201×10^9 , 2.195×10^9 , 7.999×10^8 , 2.393×10^8 cm and 8.358×10^8 cm, respectively). This could be due to a change in carrier concentration or mobility [68]. We can see that when the precursor concentration is increased to 90 mM, the resistivity values increase marginally, which could be attributed to poor crystalline characteristics. Due to imperfect atomic connections within the grain boundaries, they act as trap centers, diminishing the free charge carriers. As trapping states rise, the excess free carriers become immobilized [69]. The Arrhenius curve ($\ln(\sigma)$ vs. $1/T$) for varied molarity concentrations of WO₃ films is shown in figure 5a.

The Arrhenius Equation can be used to compute the energy of activation (E_a) [60, 70-72].

$$\sigma = \sigma_o \exp\left(\frac{-E_a}{k_B T}\right) \quad 9$$

where σ is the conductivity, σ_o represents a constant, E_a is the energy of activation, k_B represents the Boltzmann constant, and T represents the absolute temperature. The activation energy increases when the molarity concentration increases up to 80mM, which could be due to a change in stoichiometry that raises the charge carrier concentration collisions [31]. The observed value of the activation energy (E_a) decreased as concentration was increased to 90 mM. Improvements in crystallinity and film thickness were attributed to this [47]. Table 4 shows the results. For WO_3 nanofibers sprayed at varied molarity concentrations, Figure 5b shows the change in average electrical parameters and E_a . We conclude that WO_3 films deposited with 80mM have better electrical behavior than other films based on the conductivity results.

Table 4. Shown the electrical factors of WO_3 films prepared at various molarity concentration.

Molarity concentration (mM)	Resistivity (ρ) (Ωcm)	conductivity (σ_{dc}) (S cm^{-1})	Activation energy (E_a) (eV)
50	2.201×10^9	4.5428×10^{-10}	0.257
60	2.195×10^9	4.5544×10^{-9}	0.264
70	7.999×10^8	1.2501×10^{-8}	0.288
80	2.394×10^8	4.1762×10^{-8}	0.298
90	8.358×10^8	1.1964×10^{-8}	0.291

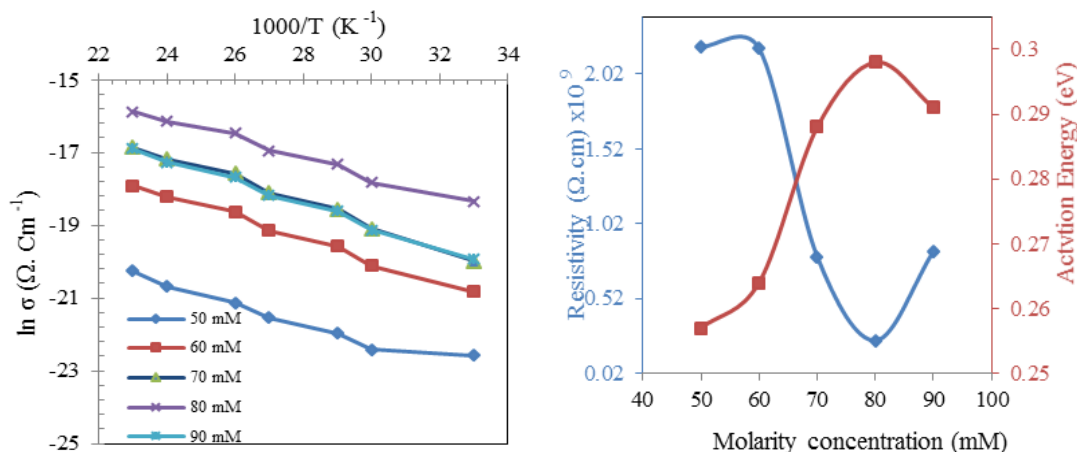


Fig. 5. (a) shows the Arrhenius curve ($\ln(\sigma)$ vs. $1/T$) for various molarity concentrations (b): electrical parameter at different molarity concentration of WO_3 film.

4. Conclusion

In summary, utilising a home-made spray apparatus, WO_3 thin films with a resistivity of 2.394×10^8 were produced on glass substrates at 350°C . XRD and DC electrical conductivity measurements were used to investigate the effect of solution concentration on film physical characteristics. The films are poly-crystalline in nature, having a monoclinic crystal structure, according to XRD analysis. The strongest peak identified in all samples is 200, according to XRD data. Other peaks were identified as (112), (202), (222), (400), (214), and (-142).

The lowest resistance and maximum conductivity ($4.1792 \times 10^8 \text{ cm}^{-1}$) were found in WO_3 thin films formed at an 80 mM concentration of solution. The favorable structural and electrical features of WO_3 thin films make them particularly excellent candidates for use in optoelectronic devices, according to these findings.

References

- [1] S. B. Ali et al., Journal of Renewable Materials, vol. 10, no 11, pp. 2819-2834, 2022; <https://doi.10.32604/jrm.2022.021609>
- [2] M. H. Mohsin et al., Journal of Renewable Materials, vol. 9, no 9, pp. 1519-1530, 2021; <https://doi.10.32604/jrm.2021.015465>.
- [3] S Basel et al., AIP Conference Proceedingsm vol. 2213, no 1, p. 020228, 2020; <https://doi.org/10.1063/5.0000185>
- [4] K. Sasikumar, R. Bharathikannan, M. Raja, Silicon, vol. 11, no. 1, pp. 137-143, 2018; <https://doi.org/10.1007/s12633-018-9938-5>
- [5] J. Kim et al., ACS applied materials & interfaces, vol. 8, no. 14, pp. 9499-9505, 2016; <https://doi.org/10.1021/acsami.5b11781>
- [6] N. N. K. Reddy, H. S. Akkera, M. C. Sekhar, S. Uthanna, Silicon, vol. 11, no. 1, pp. 159-164, 2019; <https://doi.org/10.1007/s12633-018-9840-1>
- [7] G. M. Kumar et al., RSC advances, vol. 6, no. 63, pp. 57941-57947, 2016; <https://doi.org/10.1039/C6RA10644G>
- [8] J. Semple, D. G. Georgiadou, G. Wyatt-Moon, G. Gelinck, T. D. Anthopoulos, Semiconductor Science and Technology, vol. 32, no. 12, p. 123002, 2017; <https://doi.org/10.1088/1361-6641/aa89ce>
- [9] J. Tsao et al., Advanced Electronic Materials, vol. 4, no. 1, p. 1600501, 2018; <https://doi.org/10.1002/aelm.201600501>
- [10] E.T. Salim, F.G. Khalid, M.A. Fakhri, R.S. Mahmood, Materials Today: Proceedings, vol. 42, no 5, pp. 2422-2425, 2021; <https://doi.org/10.1016/j.matpr.2020.12.551>
- [11] D. Faisal, W.K. Kalef, E.T. Salim, F.H. Alsultany, Journal of Ovonic Research, vol. 18, no 2, pp. 205–212, 2022; <https://doi.org/10.15251/JOR.2022.182.205>
- [12] Y.N. Jurn et al., Key Engineering Materials, vol. 701, pp. 57-66, 2016; <https://doi.10.4028/www.scientific.net/KEM.701.57>
- [13] M. A.Fakhri et al., Journal of Physics and Chemistry of Solids, vol. 131, pp. 180-188, 2019. <https://doi.org/10.1016/j.jpcs.2019.03.033>
- [14] A. Kadhim et al., The Scientific World Journal, vol. 2014, Article ID, p. 490951, 6 pages, 2014; <http://dx.doi.org/10.1155/2014/490951>
- [15] E. Monroy, F. Omns, F. Calle, Semiconductor Science and Technology, vol. 18, no. 4, pp. R33-R51, 2003; <https://doi.org/10.1088/0268-1242/18/4/201>
- [16] J. B. C. a. R. W. Johnson, Solid-State Electronic, vol. 39 no. 10, pp. 1409-1422, 1996; [https://doi.org/10.1016/0038-1101\(96\)00045-7](https://doi.org/10.1016/0038-1101(96)00045-7)
- [17] S. M. Max N. Yoder, IEEE Transactions on Electron Devices vol. 43, no. 10, 1996; <https://doi.org/10.1109/16.536807>
- [18] C. H. Lin and C. W. Liu, Sensors vol. 10, no. 10, pp. 8797-8826, 2010; <https://doi.org/10.3390/s101008797>
- [19] C. C. Mardare, A. W. Hassel, Physica. Status Solidi A vol. 216, no. 12, pp. 1-16, 2019; <https://doi.org/10.1002/pssa.201900047>
- [20] M. A Fakhri et al., Surface Review and Letters, vol. 26, no 10, p. 1950068, 2019; <https://doi.org/10.1142/S0218625X19500689>
- [21] J. T. Yang et al., Advanced Materials, vol. 30, no. 34, p. 1801548, 2018; <https://doi.org/10.1002/adma.201801548>

- [22] K. Qian, G. Cai, V. C. Nguyen, T. Chen, P. S. Lee, ACS applied materials & interfaces, vol. 8, no. 41, pp. 27885-27891, 2016; <https://doi.org/10.1021/acsami.6b08154>
- [23] X. Zhang et al., Scripta Materialia, vol. 189, pp. 89-94, 2020; <https://doi.org/10.1016/j.scriptamat.2020.08.012>
- [24] R.-T. Wen, C. G. Granqvist, G. A. Niklasson, Nature materials, vol. 14, no. 10, pp. 996-1001, 2015; <https://doi.org/10.1038/nmat4368>
- [25] B. Cook et al., ACS applied materials & interfaces, vol. 10, no. 1, pp. 873-879, 2018; <https://doi.org/10.1021/acsami.7b15391>
- [26] L. Li et al., Journal of Materials Chemistry, vol. 21, no. 18, pp. 6525-6530, 2011; <https://doi.org/10.1039/c0jm04557h>
- [27] A. Moudgil, V. Dhyani, S. Das, Applied Physics Letters, vol. 113, no. 10, p. 101101, 2018; <https://doi.org/10.1063/1.5045249>
- [28] S. V. Mohite, V. V. Ganbavle, K. Y. Rajpure, Journal of Alloys and Compounds, vol. 655, pp. 106-113, 2016; <https://doi.org/10.1016/j.jallcom.2015.09.154>
- [29] D. Meng et al., Journal of Alloys and Compounds, vol. 649, pp. 731-738, 2015; <https://doi.org/10.1016/j.jallcom.2015.07.142>
- [30] V. S. Vidyarthi et al., international journal of hydrogen energy, vol. 36, no. 8, pp. 4724-4731, 2011; <https://doi.org/10.1016/j.ijhydene.2011.01.087>
- [31] V. Ganbavle, S. Mohite, G. Agawane, J. Kim, K. Rajpure, Journal of colloid and interface science, vol. 451, pp. 245-254, 2015; <https://doi.org/10.1016/j.jcis.2015.04.001>
- [32] E. T. Salim et al., Iranian Journal of Science and Technology, Transactions A: Science, vol. 43, no 3, pp. 1337-1343, 2019; <https://doi.org/10.1007/s40995-018-0607-8>
- [33] Y. Al-Douri, M. A. Fakhri, A. Bouhemadou, R. Khenata, M. Ameri, Materials Chemistry and Physics, vol. 203, pp. 243-248, 2018; <https://doi.org/10.1016/j.matchemphys.2017.10.024>
- [34] E. T. Salim, J. A. Saimon, M. K. Abood, and M. A. Fakhri, Mater. Res. Express, vol. 6, no 12, p. 126459, 2019; <https://doi.org/10.1088/2053-1591/ab771c>
- [35] V. V. Ganbavle, J. H. Kim, K. Y. Rajpure, Journal of Electronic Materials, vol. 44, no. 3, pp. 874-885, 2015; <https://doi.org/10.1007/s11664-014-3618-z>
- [26] D. Meng, T. Yamazaki, Y. Shen, Z. Liu, and T. Kikuta, Applied surface science, vol. 256, no. 4, pp. 1050-1053, 2009; <https://doi.org/10.1016/j.apsusc.2009.05.075>
- [37] A. Moholkar, S. Pawar, K. Rajpure, P. Patil, and C. Bhosale, Journal of Physics and Chemistry of Solids, vol. 68, no. 10, pp. 1981-1988, 2007; <https://doi.org/10.1016/j.jpcs.2007.06.024>
- [38] S. S. Shendage et al., Journal of Analytical and Applied Pyrolysis, vol. 125, pp. 9-16, 2017; <https://doi.org/10.1016/j.jaap.2017.05.006>
- [39] V. V. Ganbavle, G. L. Agawane, A. V. Moholkar, J. H. Kim, K. Y. Rajpure, Journal of Materials Engineering and Performance vol. 23, no. 4, pp. 1204-12143, 2014; <https://doi.org/10.1007/s11665-014-0873-3>
- [40] M. A. Fakhri et al., Optik, vol. 180, pp. 768-774, 2019; <https://doi.org/10.1016/j.ijleo.2018.12.006>
- [41] M. A. Fakhri, Y. Al-Douri, U. Hashim, IEEE Photonics Journal, vol. 8, no 2, p. 4500410, 2016; <https://doi.org/10.1109/JPHOT.2016.2531583>
- [42] E. T. Salim, J. A. Saimon, M. K. Abood, M. A. Fakhri, Materials Research Express, vol. 6, no 4, p. 046420, 2019; <https://doi.org/10.1088/2053-1591/aafc7a>
- [43] S. Vanalakar et al., Ceramics International, vol. 40, no. 9, pp. 15097-15103, 2014; <https://doi.org/10.1016/j.ceramint.2014.06.121>
- [44] P. Prathap, N. Revathi, Y. P. Venkata Subbaiah, K. T. Ramakrishna Reddy, Journal of Physics: Condensed Matter, vol. 20, no. 3, 2008; <https://doi.org/10.1088/0953-8984/20/03/035205>
- [45] V. V. Ganbavle, S. V. Mohite, J. H. Kim, K. Y. Rajpure, Current Applied Physics, vol. 15, no. 2, pp. 84-93, 2015; <https://doi.org/10.1016/j.cap.2014.11.004>
- [46] M. Manickam, V. Ponnuswamy, C. Sankar, R. Suresh, Optik, vol. 127, no. 13, pp. 5278-5284,

- 2016; <https://doi.org/10.1016/j.ijleo.2016.03.008>
- [47] R. Marnadu, J. Chandrasekaran, S. Maruthamuthu, P. Vivek, V. Balasubramani, P. Balraju, *Journal of Inorganic and Organometallic Polymers and Materials*, vol. 30, no. 3, pp. 731-748, 2019; <https://doi.org/10.1007/s10904-019-01285-y>
- [48] M. S. AlWazny, E. T. Salim, B. A. Bader, M. A. Fakhry, *IOP Conference Series Materials Science and Engineering*, vol. 454, no 1, p. 012160, 2018; <https://doi.org/10.1088/1757-899X/454/1/012160>
- [49] M. A. Muhsien, E. T. Salim, I. R. Agool, *International Journal of Optics*, vol. 2013, Article ID 756402, 9 pages, 2013; <http://dx.doi.org/10.1155/2013/756402>
- [50] M. A. Fakhri, E. T. Salim, A. W. Abdulwahhab, U. Hashim, Z. T. Salim, *Optics and Laser Technology*, vol. 103, pp. 226-232, 2018; <https://doi.org/10.1016/j.optlastec.2018.01.040>
- [51] F. Hattab, M. Fakhry, 2012 First National Conference for Engineering Sciences (FNCES 2012). <https://doi.org/10.1109/NCES.2012.6740474>.
- [52] R. David Prabu, S. Valanarasu, V. Ganesh, M. Shkir, S. AlFaify, A. Kathalingam, *Surface and Interface Analysis*, vol. 50, no. 3, pp. 346-353, 2018; <https://doi.org/10.1002/sia.6374>
- [53] R. Marnadu, J. Chandrasekaran, P. Vivek, V. Balasubramani, S. Maruthamuthu, *Zeitschrift fur Physikalische Chemie*, vol. 234, no. 2, pp. 355-379, 2019; <https://doi.org/10.1515/zpch-2018-1289>
- [54] R. Marnadu, J. Chandrasekaran, M. Raja, M. Balaji, S. Maruthamuthu, P. Balraju, *Superlattices and Microstructures*, vol. 119, pp. 134-149, 2018; <https://doi.org/10.1016/j.spmi.2018.04.049>
- [55] M. A. Fakhri, E. T. Salim, M. H. A. Wahid, U. Hashim, Z. T. Salim, *Journal of Materials Science: Materials in Electronics*, vol. 29, no 11, pp. 9200-9208, 2018; <https://doi.org/10.1007/s10854-018-8948-9>
- [56] S. R. Bathe, P. S. A. Patil, *Solar Energy Materials & Solar Cells*, vol. 91, no. 12, pp. 1097-1101, 2007; <https://doi.org/10.1016/j.solmat.2007.03.005>
- [57] S. Dabbous, T. Ben Nasrallah, J. Ouerfelli, K. Boubaker, M. Amlouk, S. Belgacem, *Journal of Alloys and Compounds*, vol. 487, no. 1-2, pp. 286-292, 2009; <https://doi.org/10.1016/j.jallcom.2009.07.103>
- [58] I. N. Stranski and L. v. Krastanow, "Sitzungsberichte der akademie der wissenschaften in wien," *Akad. Wiss. Lit. Mainz Math.-Natur. Kl. Iib*, vol. 146, p. 797, 1939.
- [59] K. Shanmugasundaram, P. Thirunavukkarasu, M. Ramamurthy, M. Balaji, J. Chandrasekaran, *Oriental Journal of Chemistry*, vol. 33, no. 5, pp. 2484-2491, 2017; <https://doi.org/10.13005/ojc/330542>
- [60] M. Balaji, J. Chandrasekaran, M. Raja, *Materials Science in Semiconductor Processing*, vol. 43, pp. 104-113, 2016; <https://doi.org/10.1016/j.mssp.2015.12.009>
- [61] M. A. Fakhri et al., *The European Physical Journal Conferences*, vol. 162, p. 01005, 2017; <https://doi.org/10.1051/epjconf/201716201005>
- [62] M. K. Abood, M. H. A. Wahid, E. T. Salim, J. A. Simon, *The European Physical Journal Conferences*, vol. 162, no 12, p. 01058, 2017; <https://doi.org/10.1051/epjconf/201716201058>
- [63] Makram A. Fakhri et al., *The European Physical Journal Conferences*, vol. 162, no 7, p. 01004, 2017; <https://doi.org/10.1051/epjconf/201716201004>
- [64] A. Al-Mohammad, *physica status solidi (a)*, vol. 205, no. 12, pp. 2880-2885, 2008; <https://doi.org/10.1002/pssa.200723232>
- [65] M. Raja, J. Chandrasekaran, M. Balaji, *Optik - International Journal for Light and Electron Optics*, vol. 127, no. (22), pp. 11009-11019, 2016; <https://doi.org/10.1016/j.ijleo.2016.08.079>
- [66] S. Shinde, P. Shinde, C. Bhosale, K. Rajpure, *Journal of Physics D: Applied Physics*, vol. 41, no. 10, p. 105109, 2008; <https://doi.org/10.1088/0022-3727/41/10/105109>
- [67] H. Attouche, S. Rahmane, S. Hettal, N. Kouidri, *Optik*, vol. 203, 2020; <https://doi.org/10.1016/j.ijleo.2019.163985>

- [68] A. Abdelkrim, S. Rahmane, O. Abdelouahab, A. Hafida, K. Nabila, Chinese Physics B, vol. 25, no. 4, p. 046801, 2016; <https://doi.org/10.1088/1674-1056/25/4/046801>
- [69] N. Anitha, M. Anitha, J. R. Mohamed, S. Valanarasu, L. Amalraj, Journal of Asian Ceramic Societies, vol. 6, no. 2, pp. 121-131, 2018; <https://doi.org/10.1080/21870764.2018.1450026>
- [70] M. A. Fakhri et al., Journal of Materials Science: Materials in Electronics, vol. 28, no 22, pp. 16728-16735, 2017; <https://doi.org/10.1007/s10854-017-7586-y>
- [71] M. A. Muhsien, E. T. Salim, Y. Al-Douri, A. F. Sale, I. R. Agool, Applied Physics A, vol. 120, no 2, pp. 725-730, 2015; <https://doi.org/10.1007/s00339-015-9249-2>
- [72] M. A. Muhsien, E. T. Salem, I. R. Agool, H. H. Hamdan, Appl. Nanoscience, vol. 4, pp. 719–732, 2014; <https://doi.org/10.1007/s13204-013-0244-7>